Desalination and Water Treatment
www.deswater.com

doi: 10.1080/19443994.2015.1025433

57 (2016) 8639–8648
April

Taylor & Francis
Taylor & Francis Group

Fabrication of polyamide membrane reached by $MgTiO_3$ nanoparticles for ground water purification

A.S. AL-Hobaib[a], J. El Ghoul[b,c,*], L. El Mir[b,c]

[a]*Institute of Atomic Energy Research, King Abdulaziz City for Science And Technology (KACST), P.O. Box 6086, 11442 Riyadh, Saudi Arabia*
[b]*Department of Physics, College of Sciences, Al Imam Mohammad Ibn Saud Islamic University (IMSIU), Riyadh 11623, Saudi Arabia, emails: jaber.elghoul@fsg.rnu.tn, ghoultn@yahoo.fr (J. El Ghoul)*
[c]*Laboratory of Physics of Materials and Nanomaterials Applied at Environment (LaPhyMNE), Faculty of Sciences in Gabes, Gabes University, Gabes, Tunisia*

Received 14 March 2014; Accepted 24 February 2015

ABSTRACT

Here, we report the fabrication of mixed matrix reverse osmosis membranes by interfacial polymerization (IP) of nanocomposite on porous polysulfone supports. Nanocomposites elaborated for this study comprise magnesium titanium oxide ($MgTiO_3$) nanoparticles dispersed in polyamide host matrix synthesized by the *in situ* IP process on porous polysulfone commercial supports. Aqueous m-phenyl diamine and organic trimesoyl chloride nanoparticles mixture solutions were used in the IP process. Nanoparticles of $MgTiO_3$ with a size of about 80 nm were used as filler for the fabrication of the nanocomposite membranes with a concentrations varying from 0.0001 to 0.009 wt.%. The samples were characterized by X-ray diffraction, scanning electron microscopy, atomic force microscopy, and contact angle setup. Their performances were evaluated based on the water permeability and salt rejection. Results indicated that the nanoparticles are well dispersed in the host matrix of polyamide layer and improved membrane performance under optimal nanoparticle content. By changing the concentration of the filler, hydrophilicity and roughness of the nanocomposite membranes were increased. Notably, the permeate water flux increased from 26 to 44.6 L/m^2 h at the nanoparticles concentration of 0.001% with the maintaining of high salt rejection of 98%. These results were obtained with initial NaCl concentration of 2,000 ppm and under pressure of 225 psi. Also better hydrophilicity was obtained; the contact angle was decreased from 73 to 24°.

Keywords: Nano-$MgTiO_3$; Interfacial polymerization; Nanocomposite; Nanofiltration; Desalination

1. Introduction

The growing demand for fresh water and the remarkable water crisis have spurred enormous interest in energy efficient technologies to produce safe drinking water from the ocean. Membrane filtration based on reverse osmosis (RO) is one of the most promising ways to desalinate seawater or brackish water, and thin film composite (TFC) membranes, comprised of ultrathin active layers upon porous

*Corresponding author.

supports, have been widely used for this application [1–3]. Due to their completely hydrophilic characteristic and their certain functionality to benefit membrane properties of fouling reduction, inorganic materials incorporation into the polymer matrix is being of great interest [4]. Therefore, extensive efforts are being devoted to incorporate inorganic nanoparticles (NPs) into polymeric membrane. It was reported that inorganic materials could be incorporated into membranes by doping and coating technologies [5–8]. However, the doping technology has the disadvantage that inorganic materials are buried in the polymer matrix and in turn rendered non-functional. On the other hand, the coating technology has the disadvantage of the instability of inorganic materials onto polymer surface, especially for those not subject to chemical bonds or physical restraints between the inorganic materials and membrane matrix. The concept for formation of mixed matrix RO membranes, by interfacial polymerization (IP) of nanocomposite thin films on porous supports, has been reported [9,10]. The emergence of nanotechnology in membrane materials science could offer an attractive alternative to polymeric materials [11,12]. Titanium oxide nanoparticles have been incorporated into polyamide (PA) thin film membranes by applying an *in situ* IP procedure [13]. Polyethersulfone—TiO_2 nanoparticles composite membranes made from casting solution consisting of various compositions of polymer solvents (DMF and EtOH) and TiO_2 additive showed significant improvement in fouling resistance [14]. Silica oxide nanoparticles have been incorporated into PA thin film membrane via *in situ* IP process [7,15]. Zeolite nanoparticles have been used to prepare nanocomposite membrane where first zeolite nanoparticles are synthesized via a template hydrothermal reaction followed by a series of complex processes involving template removal, carbonization, sodium exchange, and calcination [16]. Zirconium oxide has been used as a bulk material in polyvinylidene fluoride membranes [17]. ZnO enhanced polyethersulfone membrane has been synthesized by diffusion induced phase inversion in N-methyl-pyrrolidone. It has reported that membrane materials enriched by ZnO nanoparticles have significantly improved membrane features. It showed lower flux decline and better permeability compared to neat polymeric membrane due to a higher hydrophilicity of the ZnO membranes. ZnO nanoparticles provide a remarkable improvement in the methylene blue rejection potential [18]. Aluminum oxide (Al_2O_3) nanoparticles were also incorporated into a membrane of polyvinylidene fluoride using dimethyl acetamide as solvent [19]. Same type of polymer was used to prepare a membrane by doping with anhydrous and hydrated aluminum oxide particles through *in situ* particles embedment and subsequent crystal growth under a hydrothermal environment [20]. Furthermore, another issue that can limit the application of nanoparticles is their toxicity since it is thought that nanoparticles may persist as small particles in aquatic systems and then their bioavailability could be significantly greater than that of larger particles.

The novelty of this paper is the incorporation of $MgTiO_3$ nanoparticles in membranes in order to significantly enhance the performance of nanofiltration technology in terms of permeation and rejection. The eventual membrane structure was also studied in this work.

2. Experimental

2.1. Preparation of the nanocomposite membranes

A PS-20 (polysulfone supports) membrane was immersed in deionized water (DI) during 4 h, then removed from the water and positioned on a plastic plate. One hundred milliliter of 2% (w/v, i.e. g MPD/100 mL water) m-phenyl diamine (MPD) (1,3-Phenylendiamine, >99%) solution was poured into the frame and allowed to contact the PS membrane for at least 5 min before draining the excess MPD solution. This residence time allowed MPD to at least partially penetrate into the pores of the porous support. Residual droplets of solution on the top surface of the PS membrane were removed by rolling a rubber roller across the membrane surface one time. Consistent with previous literature reports, the rubber roller was firmly pressed against the membrane surface to ensure that no visible aqueous droplets, which could form defects if left on the membrane, remained following the rolling process [21,22]. Afterwards, the PS membrane was placed in 80 mL of 0.1% (w/v) trimesoyl chloride (TMC) (1,3,5-benzenetricarbonyl trichloride, >98%)/n-hexane solution. After 1 min, the TMC/n-hexane solution was drained. The membrane surface was rinsed using Na_2CO_3 to wash away residual reagents, and the membrane was dried in air at ambient conditions for 1 min. Finally, the entire membrane was immersed in DI water until use. The nanocomposite membranes were made by dispersing 0.0001–0.009 g of commercial $MgTiO_3$ (Aldrich, >99%) in the TMC/hexane solution by ultrasonication for 1 h at room temperature. Then, TFNC membranes were prepared by keeping the mass of the added $MgTiO_3$ at 0.001 g and varying the concentration of MPD and TMC in the range of 1–3% (w/v) and 0.05–0.2%, respectively.

2.2. Characterization

The crystalline phases of the nanopowders were identified by X-ray diffraction (XRD) using a Bruker D5005 powder X-ray diffractometer. The morphology and microstructure of the powders and as-synthesized nanocomposite membranes were examined by the means of scanning electron microscope (SEM, FEI Nova-Nano SEM-600, Netherlands). The quantitative analysis of the membranes was performed by energy dispersive X-ray spectroscopy (EDX) setup. In addition, atomic force microscopy (AFM) was used to analyze the surface morphology and roughness of the prepared membranes. The AFM device was Nanosurf scanning probe-optical microscope (Bruker Corporation). Small squares of the prepared membranes (approximately 1 cm^2) were cut and glued on glass substrate.

Contact angle analysis was performed using a Ramé-Hart Model 250 Standard Goniometer/Tensiometer with DROP image advanced software (Ramé-Hart Instrument Co., Succasunna, NJ 07876 USA). A water droplet was placed on a dry flat homogeneous membrane surface and the contact angle between the water and membrane was measured when no further change was observed. The average contact angle for distilled water was determined in a series of eight measurements for each of the different membrane surfaces.

2.3. Membrane filtration experiments

The performance of the prepared membranes was analyzed through a cross-flow system (CF042SS316 Cell, Sterlitech Corp.) The valid membrane area in this system was 42 cm^2. The feed temperature was 25°C with pH adjusted between 6 and 7. The filtration was carried out at the pressure of 225 psi and the stirring speed was of 2,000 rpm. All measurements of the water flux and salt rejection were measured after 30 min of water filtration experiments to ensure that had reached stability. The flux was calculated by Eq. (1):

$$J = \frac{V_p}{A \times t} \tag{1}$$

where J is the water flux (L/m^2 h), V_p is the permeate volume (L), A is the membrane area (m^2), and t is the treatment time (h).

The salt rejection was measured by Eq. (2):

$$R = \left(1 - \frac{C_p}{C_f}\right) \times 100 \tag{2}$$

where R is the rejection ratio, C_p and C_f are the salt concentrations of permeate and feed, respectively.

3. Results and discussion

3.1. Characterization of the $MgTiO_3$ powders

The $MgTiO_3$ powders were characterized by XRD, SEM, and EDX. Fig. 1 shows typical XRD spectrum of the powder after thermal treatment. We noticed the appearance of nine pronounced diffraction peaks characteristics of $MgTiO_3$ [23]. The average grain size can be calculated using the Debye–Scherrer formula (Eq. (3)) [24]:

$$G = 0.9\lambda / B \cos\theta_B \tag{3}$$

where λ is the X-ray wavelength (1.5418 Å), θ_B is the maximum of the Bragg diffraction peak, and B is the linewidth at half maximum. After a correction for the instrumental broadening, the obtained average value of the crystallites is 80 nm. Fig. 2 shows the surface morphology and EDX analysis of nano-$MgTiO_3$. An estimate of the grain size indicates that they are in the form of nanocrystallites with a dimension around 80 nm. The EDX analysis during the SEM observation confirms that the presence of Mg and Ti, in good agreement with XRD results.

3.2. Membrane characterizations and performances

The synthesized membranes surfaces were observed by SEM accompanied by EDX system. After

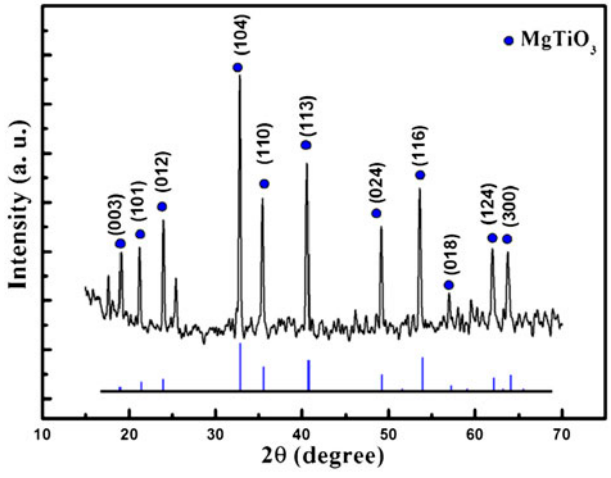

Fig. 1. XRD patterns of $MgTiO_3$ nanoparticles.

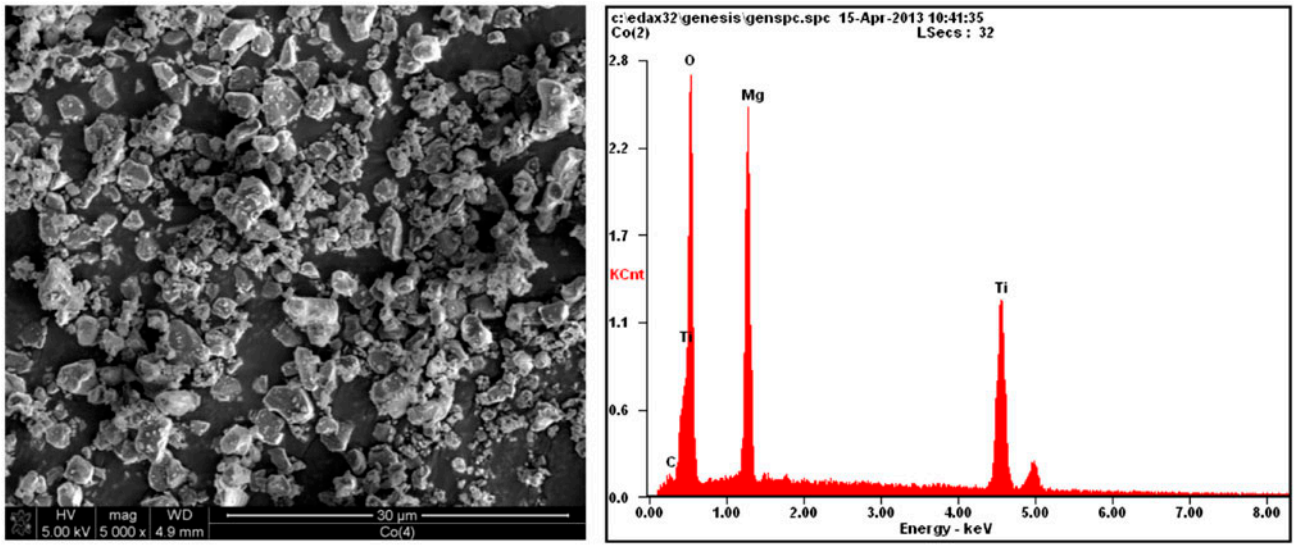

Fig. 2. SEM and EDX images of $MgTiO_3$ nanoparticles.

the IP process, the TFC membranes coated on the PS support layer by the reaction between MPD and TMC have led to a leaf-like morphology (Fig. 3(a)). The impregnation of $MgTiO_3$-NPs does not have a great effect in micrometric scale on the overall morphology of TFC in the tested weight range (Fig. 3(b)). The difference between the samples is translated by the EDX quantitative analysis showing the presence of carbon, oxygen, magnesium, and titanium peaks as component elements. In comparison, TFN membrane exhibits ascendant and broaden ridge–valley structure, which suggest variation on surface roughness of TFN membranes under different nano-$MgTiO_3$ loadings (Fig. 4(a)–(d)). AFM was used to further analyze the morphology of membrane surface. As shown in Fig. 4, the TFC membrane showed much higher surface roughness (31 nm) due to the leaf-like shape of the PS support. The RMS value increased to 72 nm in the TFNC-0.009 membrane, which could be caused by the presence of $MgTiO_3$-NPs on the membrane surface.

Our membranes were subjected to contact angle measurements. Standard deviations obtained on a single sample are of the order of a few degrees, which represent an acceptable reproducibility. Fig. 5 shows the measurements of the contact angle for the various weights of $MgTiO_3$ nanoparticles. The remarkable conclusion from Fig. 5 is the important decay of the contact angle from 73˚ (control TFC membrane) to about 24˚ after addition 0.001 g of $MgTiO_3$ nanoparticles into TFC membrane. It is known that there is a strong correlation between the orientation (geometry) of water at a solid–liquid interface and the hydrophilicity of the solid surface [25,26]. The restructuring of interfacial water molecules can explain the increase of the hydrophilicity. The increased ordering of the interfacial water molecules improves the water molecule's ability to form hydrogen bonds and, in turn, produces stronger interactions between water and the solid phase (TFC surface). In fact, the addition of $MgTiO_3$ increases the hydrophilicity of the membrane as a result of the high affinity of nanoparticles to water. This observation can be explained by the presence of hydrophilic $MgTiO_3$ nanoparticles in membrane structures, and the contact angle should be lower because a larger fraction of water diffuses through the membrane structure.

To conclude, the fall of the contact angle with the addition of nanoparticles in the membrane could be caused by two reasons. First, the embedded spherical $MgTiO_3$ NPs can be exposed on the membrane surface. Therefore, the membrane surface hydrophilicity may increases because of the hydrophilic properties of these NPs. Enriched by $MgTiO_3$ NPs, the membrane surface could even become more hydrophilic due to the capability of the hydrophilic pores to imbibe water via capillary effects [27]. This is consistent with the result by Jeong et al. [9], who observed that the contact angle of membrane surface decreased with increasing Zeolite concentration and attributed this to the superhydrophilic property of Zeolite. Second, the fact that NPs may hydrate and release heat when contacting with MPD aqueous solution [28]. This process can affect the IP reaction between MPD and TMC, and subsequently the chemical structure of the PS support. If more number of the acyl chloride groups in TMC

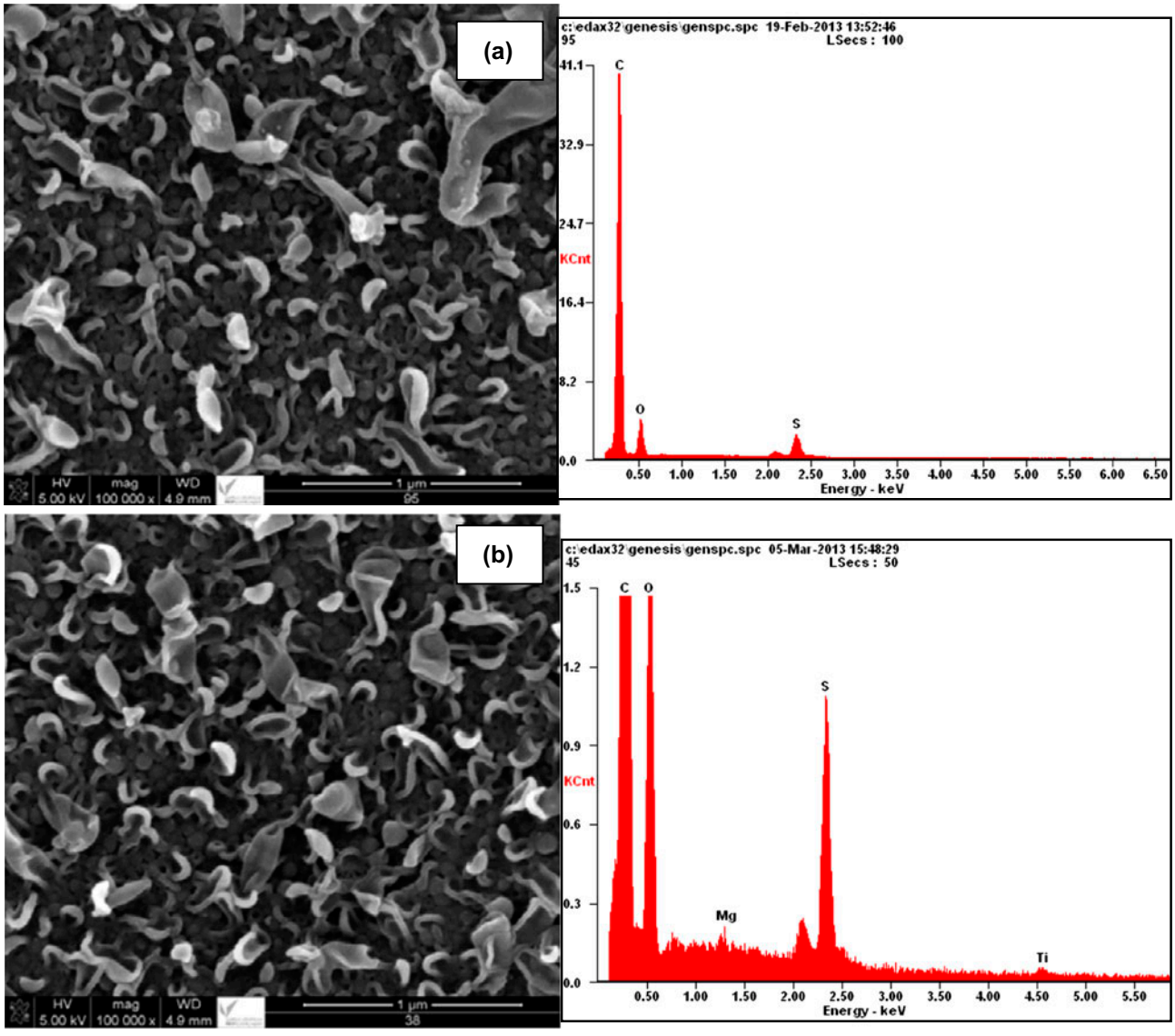

Fig. 3. EDX and SEM images of membranes surface morphologies: (a) TFC and (b) TFNC-0.001.

remained on the surface without reaction with amine groups, the hydrolysis of acyl chloride could generate carboxylic acid functional groups, then the surface hydrophilicity increased [29]. Hydrophilic nano-$MgTiO_3$ significantly improves the hydrophilicity of the membranes. It is known that hydrophilicity is favorable for improving the water flux and antifouling ability.

It has been shown that the structure and hydrophilicity of the membrane are the two main factors that govern the filtration properties of membranes. The presence of hydrophilic nano-$MgTiO_3$ improves the hydrophilicity of membranes, which is much favorable to the water flux. Consequently, improved hydrophilicity and membrane structure contribute to enhance the water flux of hybrid membrane compared to TFC membrane [30]. The filtration properties of membranes have been obtained using the cross-flow system at 25°C. Fig. 6 presents the water fluxes and the salt rejection of the prepared membranes. As the weight of added nano-$MgTiO_3$ increases, the water flux of the membrane increases to a peak value and then begins to decrease. The $MgTiO_3$/TFC hybrid membrane exhibits the highest water flux of 44.6 L/m^2 h at nano-$MgTiO_3$ concentration of 0.001 g. This flux represents an improvement of about 73% over that of the TFC membrane. The salt rejection ratios of all prepared membranes were unchanged. When the weight of

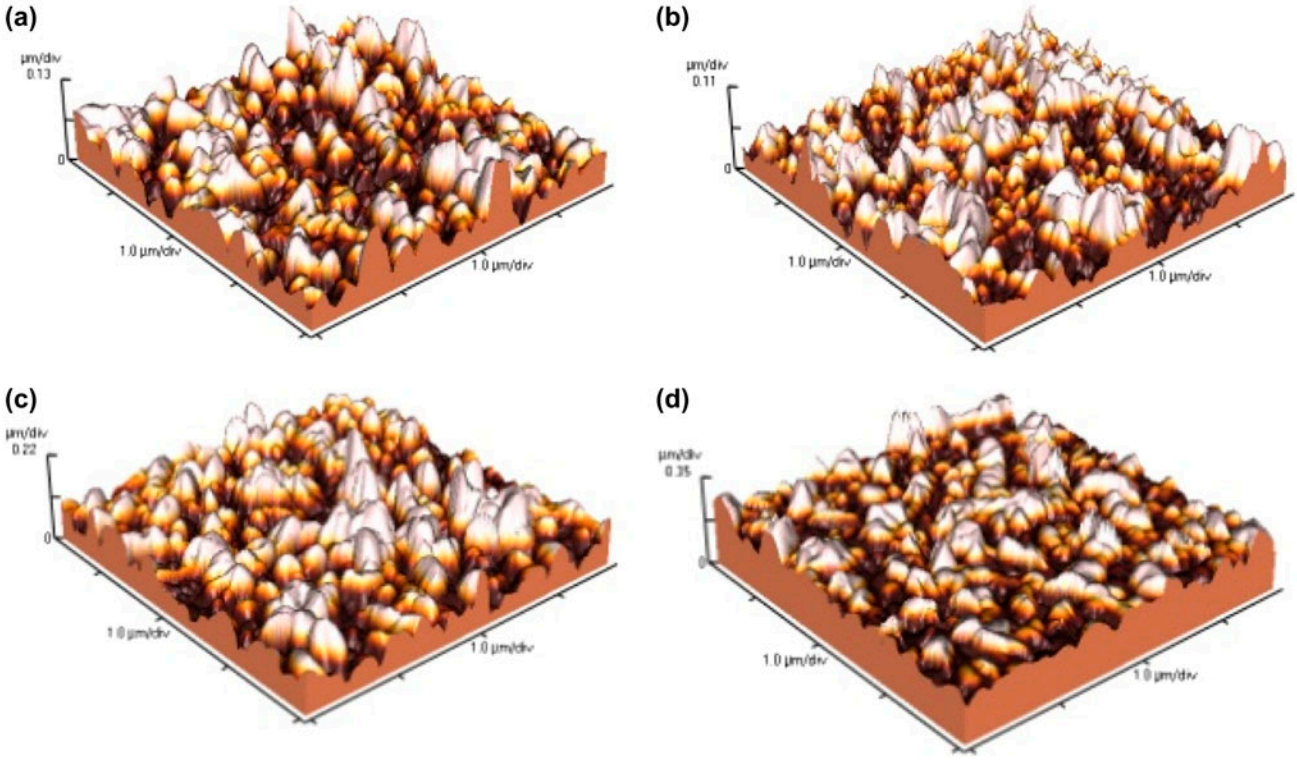

Fig. 4. AFM images of (a) TFC, (b) TFNC-0.001, (c) TFNC-0.003, and (d) TFNC-0.009 membranes.

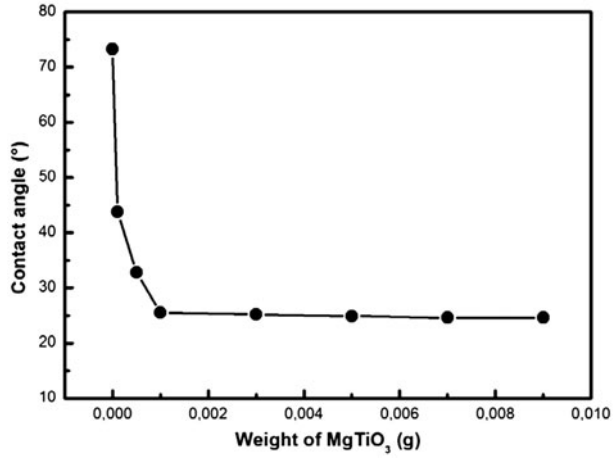

Fig. 5. Contact angle variation with the increasing weight of the added nano-$MgTiO_3$.

added nano-$MgTiO_3$ exceeds 0.001 g, the water flux begins to decrease. This phenomenon is the synergetic result of decreased porosity and/or aggregation of nano-$MgTiO_3$.

There are many literature reports regarding the performance of IP of commercial polyamide TFC membranes and aromatic polyamide TFC desalination membranes based on MPD and TMC [31,32]. The permeate flux of RO membranes is reported to be influenced by the thickness, hydrophilicity, and density of the polyamide barrier layer [33,34]. Linkages between film thickness, structure, and membrane performance have been studied experimentally and simulated by mathematical models [35–37]. Generally, IP of MPD and TMC is believed to involve an incipient fast stage that forms a dense core barrier layer followed by a slow growth stage that is monomer diffusion limited [35,36]. The fast reaction upon contact of both monomers at the oil–water interface in the incipient stage provides the dense core layer that is significantly thinner than the extended loose layer formed later as monomer diffuses through the dense core layer [37]. Freger [36] showed that the thickness of the dense core layer decreases as the concentration of either monomer increases. However, the overall polyamide layer thickness may evolved differently to increases in monomer concentration because increased MPD concentration may improve the driving force for diffusion of the MPD into the organic phase, which increases the polyamide thickness during the slow-growth stage. For example, Chai and Krantz [35] found that the film thickness increase is accompanied by an increased concentration of amine, and permeate flux

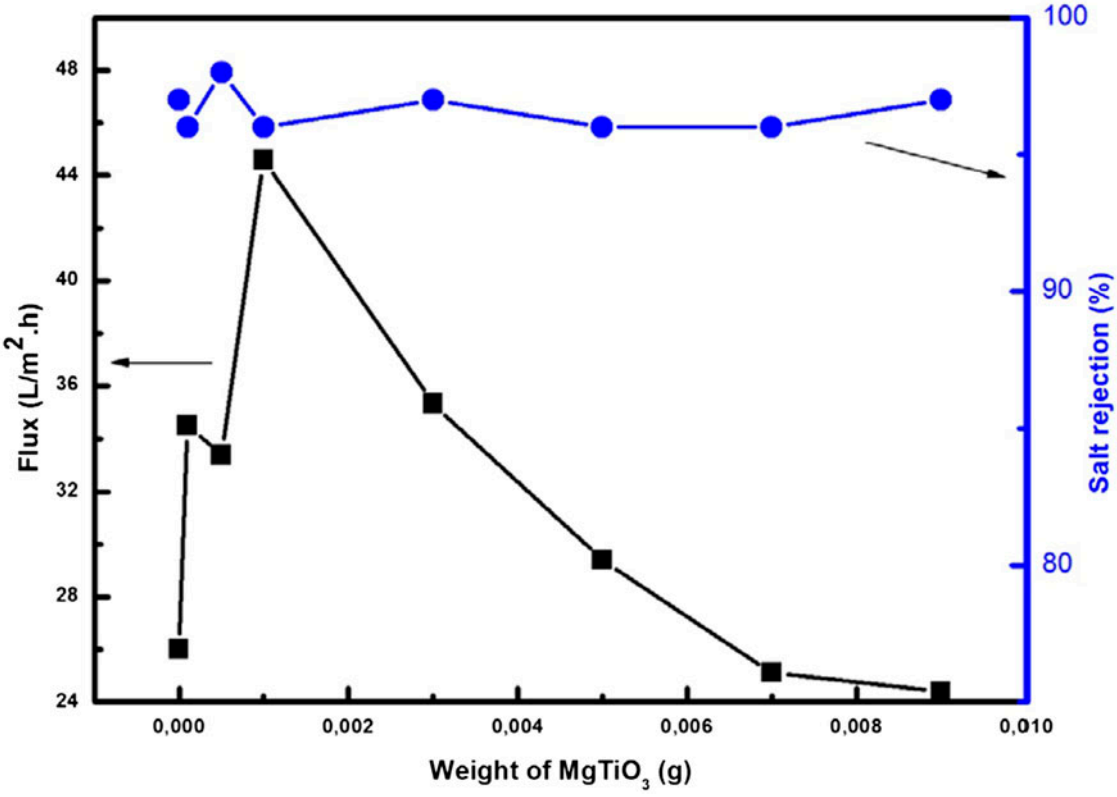

Fig. 6. Flux and rejection variation with the increasing weight of the added nano-$MgTiO_3$.

would typically decrease as polyamide layer thickness increased and vice versa. The polymer density across the barrier layer is not uniform [38]. The core layer (near the original MPD/TMC interface) is the most dense region, and the polymer density decreases gradually as the polymer grows further into the organic phase [36,39]. In many applications of IP using MPD and TMC, the initial amine concentration is much higher than the acyl chloride concentration. Either decreasing the amine concentration or increasing the acyl chloride concentration (thereby bringing the molar ratio of amine to acid chloride groups closer to unity) results in a denser polyamide layer compared to those prepared using higher amine/acid chloride molar ratios [40]. Increases in either the density or thickness of the MPD/TMC barrier layer should increase the mass transfer resistance of the resulting membrane, thereby reducing permeate flux. Thus, varying the initial concentration of monomers can influence the membrane's water and salt transport properties. Table 1 illustrates the comparison between the obtained membrane transport properties of the optimum conditions corresponding to 2% MPD and 0.1% TMC, to those of the membranes enriched by different nanoparticles reported in the literature. TFNC membranes were prepared by varying the concentration of MPD and TMC and keeping the mass of added $MgTiO_3$ at 0.001 g. The obtained results seem to be very promising compared to the published ones. The influences of MPD and TMC concentrations on permeate flux and salt passage are presented in Figs. 7 and 8, respectively. To assist in the discussion below, the molar ratio of amine groups on the MPD to the acid chloride (i.e. acyl chloride) groups on the TMC based on the concentrations of MPD and TMC used in the polymerization process is reported in these figures. All membranes exhibited salt passage values of less than 3% (i.e. rejection >97%), but permeate flux varied significantly.

Fig. 7 shows the influence of MPD concentration on salt passage and permeates flux. Salt passage was relatively insensitive to MPD concentration over the range of concentrations considered, suggesting the formation of defect-free (or at least nearly defect-free) membranes in all cases. Permeate flux exhibited a maximum near 2% (w/v) MPD. As MPD concentration increases, the driving force for MPD diffusion into the organic phase expand; increased MPD concentration could, therefore, increase the barrier layer thickness and, thus lower permeate flux. As MPD concentration decreases, layer

Table 1
Performance of polyamide thin film nanocomposite membranes

Nanoparticles type	Salt rejection (%)	Flux L/m^2 h	References
TFC (225 psi; 1,500 ppm)	99.6	40	[21]
TFC (225 psi; 2,000 ppm)	99.5	43	[21]
TFC (225 psi; 2,000 ppm)	99.5	44	[21]
$MgTiO_3$ nanoparticles/TFC (225 psi; 2,000 ppm)	98	45	This work
TiO_2 nanoparticles/TFC (225 psi; 2,000 ppm)	96.6	24.5	[5]
Zeolite nanoparticles/TFC (225 psi; 2,000 ppm)	93	40.2	[9]
Silica nanoparticles and TEOS hydrolyzed silica/TFC (225 psi; 2,000 ppm)	71.7	40.8	[15]
Silica nanoparticles/TFC (225 psi; 2,000 ppm)	91	27.2	[31]
Al_2O_3 nanoparticles/TFC (225 psi; 2,000 ppm)	88	5	[32]

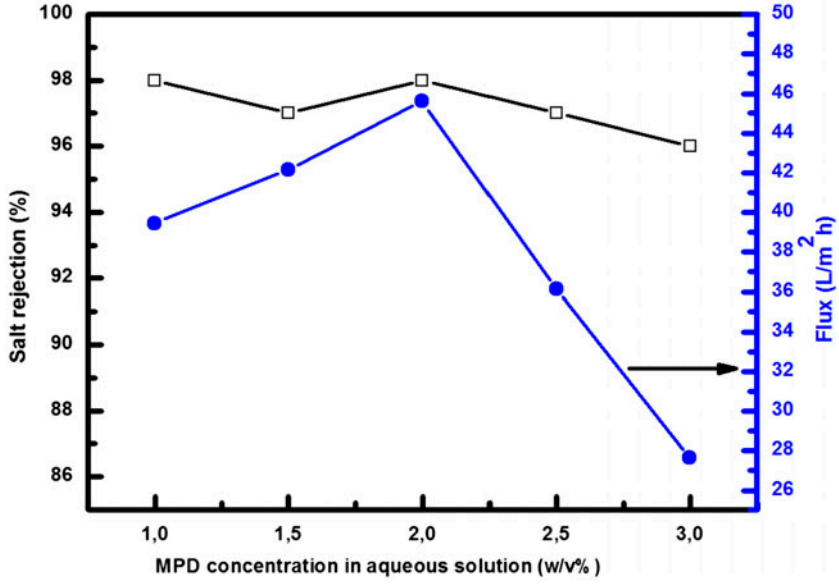

Fig. 7. Dependence of polyamide TFC membrane performance on MPD concentration.

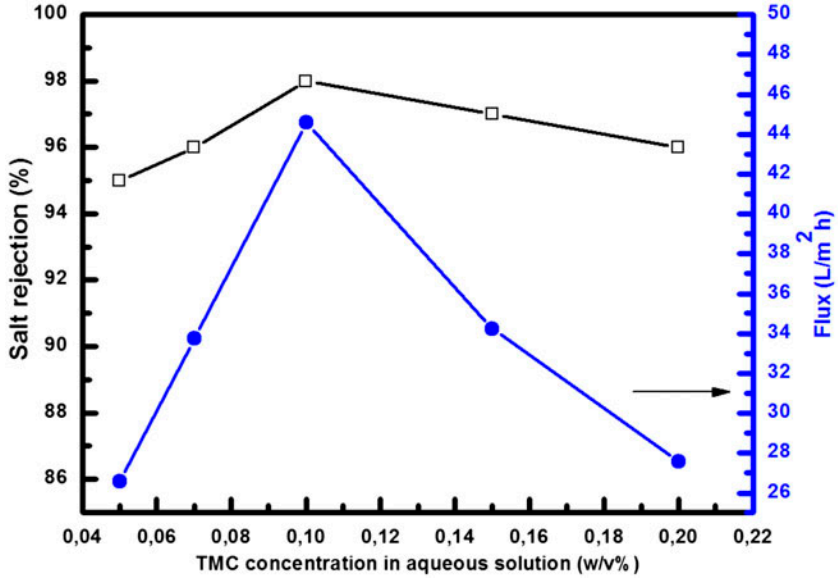

Fig. 8. Dependence of polyamide TFC membrane performance on TMC concentration.

thickness is expected to decrease, which would tend to increase the flux, but the resulting layer is expected to become more dense as the molar ratio of amine/acyl chloride becomes closer to unity, which would lower flux [36,41]. Based on what is potentially a complex interplay between these phenomena, a maximum in permeate flux was observed.

Fig. 8 illustrates the influence of TMC concentration in the organic phase on permeate flux and salt passage when the MPD concentration in the aqueous phase was held constant at 2% (w/v), which is near the optimum value observed in Fig. 7. Since IP is typically MPD diffusion controlled during growth of the polyamide layer, variations in TMC concentration would affect the layer density by varying the amine/acyl chloride molar ratio [36,41]. As TMC concentration increases, the amine/acyl chloride molar ratio decreases, which is expected to increase film density, resulting in lower permeate flux [36,41]. However, a decrease in permeate flux was also observed at the lowest TMC concentration. At this range of TMC concentration (<0.1%), the IP reaction is reported to be TMC diffusion limited [35]. A low concentration of acyl chloride groups in the reaction zone may allow the polyamide film to grow thicker, which would decrease the flux [28].

4. Conclusion

The $MgTiO_3$ NPs were embedded, with different weights, into polyamide membrane via IP process. The NPs strongly affects the properties of the membrane. EDX confirms the incorporation of the $MgTiO_3$ nanoparticles into the polyamide membrane. The contact angle of the membrane decreases from 73 to 24° for the sample with NPs content of about 0.001 g. With the increased weight of the added nano-$MgTiO_3$, the flux improves and the contact angle varies very slightly. The TFNC hybrid membrane exhibits the highest water flux of about 45 L/m^2 h for NPs content of 0.001 g; this flux represents an improvement of 73% relative to that of the TFC membrane and seems to be very promising compared to the published results. In addition, the rejection of the TFNC membrane is not obviously changed.

References

[1] R.J. Petersen, Composite reverse-osmosis and nanofiltration membranes, J. Membr. Sci. 83 (1993) 81–150.

[2] M. Wilf, The Guidebook of Membrane Desalination Technology: Reverse Osmosis, Nanofiltration and Hybrid Systems: Process, Design, Applications and Economics, Balaban Desalination Publications, L'Aquila, 2007.

[3] N. Niksefat, M. Jahanshahi, A. Rahimpour, The effect of SiO_2 nanoparticles on morphology and performance of thin film composite membranes for forward osmosis application, Desalination 343 (2014) 140–146.

[4] X. Wang, X. Li, K. Shih, In situ embedment and growth of anhydrous and hydrated aluminum oxide particles on polyvinylidene fluoride (PVDF) membranes, J. Membr. Sci. 368 (2011) 134–143.

[5] S.Y. Kwak, S.H. Kim, S.S. Kim, Hybrid organic/inorganic reverse osmosis (RO) membrane for bactericidal anti-fouling. 1. Preparation and characterization of TiO2 nanoparticle self-assembled aromatic polyamide thin-film-composite (TFC) membrane, Environ. Sci. Technol. 35 (2001) 2388–2394.

[6] D.J. Lin, C.L. Chang, F.M. Huang, L.P. Cheng, Effect of salt additive on the formation of microporous poly (vinylidene fluoride) membranes by phase inversion from $LiClO_4$/water/DMF/PVDF system, Polymer 44 (2003) 413–422.

[7] M. Ben-Sasson, X. Lu, E. Bar-Zeev, K.R. Zodrow, S. Nejati, G. Qi, E.P. Giannelis, M. Elimelech, In situ formation of silver nanoparticles on thin-film composite reverse osmosis membranes for biofouling mitigation, Water Res. 62 (2014) 260–270.

[8] B. Rajaeian, A. Rahimpour, M.O. Tade, S. Liu, Fabrication and characterization of polyamide thin film nanocomposite (TFN) nanofiltration membrane impregnated with TiO_2 nanoparticles, Desalineation 313 (2013) 176–188.

[9] B.H. Jeong, E.M.V. Hoek, Y. Yan, A. Subramani, X. Huang, G. Hurwitz, A.K. Ghosh, A. Jawor, Interfacial polymerization of thin film nanocomposites: A new concept for reverse osmosis membranes, J. Membr. Sci. 294 (2007) 1–7.

[10] Q. Wang, G.S. Zhang, Z.S. Li, S. Deng, H. Chen, P. Wang, Preparation and properties of polyamide/titania composite nanofiltration membrane by interfacial polymerization, Desalination 352 (2014) 38–44.

[11] Md.S. Rahaman, H.T. Aubin, M. Ben-Sasson, C.K. Ober, M. Nielsen, M. Elimelech, Control of biofouling on reverse osmosis polyamide membranes modified with biocidal nanoparticles and antifouling polymer brushes, J. Mater. Chem. B, 2 (2014) 1724–1732.

[12] K.P. Lee, T.C. Arnot, D. Mattia, A review of reverse osmosis membrane materials for desalination—Development to date and future potential, J. Membr. Sci. 370 (2011) 1–22.

[13] S.H.S. Lee, J. Im, J.H. Kim, H.J. Kim, J.P. Kim, B.R. Min, Polyamide thin-film nanofiltration membranes containing TiO_2 nanoparticles, Desalination 219 (2008) 48–56.

[14] A. Sotto, A. Boromand, R. Zhang, P. Luis, J.M. Arsuaga, J. Kim, B. Van der Bruggen, Effect of nanoparticle aggregation at low concentrations of TiO_2 on the hydrophilicity, morphology, and fouling resistance of PES–TiO_2 membranes, J. Colloid Interface Sci. 363 (2011) 540–550.

[15] G.L. Jadav, P.S. Singh, Synthesis of novel silica polyamide nanocomposite membrane with enhanced properties, J. Membr. Sci. 328 (2009) 257–267.

[16] M.L. Lind, A.K. Ghosh, A. Jawor, X. Huang, W. Hou, Y. Yang, E.M.V. Hoek, Influence of zeolite crystal size on zeolite-polyamide thin film nanocomposite membranes, Langmuir 25 (2009) 10139–10145.

[17] A. Bottino, G. Capannelli, A. Comite, Preparation and characterization of Novel porous PVDFe ZrO_2 composite membranes, Desalination 14 (2000) 35–40.
[18] S. Balta, A. Sotto, P. Luis, L. Benea, B. Van der Bruggen, J. Kim, A new outlook on membrane enhancement with nanoparticles: The alternative of ZnO, J. Membr. Sci. 389 (2012) 155–161.
[19] L. Yan, Y.S. Li, C.B. Xiang, Preparation of poly(vinylidene fluoride) (PVDF) ultrafiltration membrane modified by nano-sized alumina (Al_2O_3) and its antifouling research, Polymer 46 (2005) 7701–7706.
[20] X.O. Wang, X.Y. Li, K. Shih, In situ embedment and growth of anhydrous and hydrated aluminum oxide particles on polyvinylidene fluoride (PVDF) membranes, J. Membr. Sci. 368 (2011) 134–143.
[21] W. Xie, G.M. Geise, B.D. Freeman, H.-S. Lee, G. Byun, J.E. McGrath, Polyamide interfacial composite membranes prepared from m-phenylene diamine, trimesoyl chloride and a new disulfonated diamine, J. Membr. Sci. 403–404 (2012) 152–161.
[22] S.D. Arthur, Method for Manufacturing of Multilayer Reverse Osmosis Membrane of Polyamide-urea, US Patent 5,084,182, 1992.
[23] Y. Yuan, S.R. Zhang, X.H. Zhou, E.Z. Li, $MgTiO_3$ filled PTFE composites for microwave substrate applications, Mater. Chem. Phys. 141 (2013) 175–179.
[24] B.D. Cullity, Elements of X-ray Diffractions, Addison-Wesley, Reading, MA, 1978, pp. 102–110.
[25] G. Hurwitz, G.R. Guillen, E.M.V. Hoek, Probing polyamide membrane surface charge, zeta potential, wettability, and hydrophilicity with contact angle measurements, J. Membr. Sci. 349 (2010) 349–357.
[26] Q. Du, E. Freysz, Y.R. Shen, Surface vibrational spectroscopic studies of hydrogen bonding and hydrophobicity, Science 264 (1994) 826–828.
[27] J.H. Li, Y.Y. Xu, L.P. Zhu, J.H. Wang, C.H. Du, Fabrication and characterization of a novel TiO_2 nanoparticle self-assembly membrane with improved fouling resistance, J. Membr. Sci. 326 (2009) 659–666.
[28] M.L. Lind, A.K. Ghosh, A. Jawor, X. Huang, W. Hou, Y. Yang, E.M.V. Hoek, Influence of zeolite crystal size on zeolite-polyamide thin film nanocomposite membranes, Langmuir 25 (2009) 10139–10145.
[29] C.K. Kim, J.H. Kim, I.J. Roh, J.J. Kim, The changes of membrane performance with polyamide molecular structure in the reverse osmosis process, J. Membr. Sci. 165 (2000) 189–199.
[30] H. Wu, B. Tang, P. Wu, Novel ultrafiltration membranes prepared from a multi-walled carbon nanotubes/polymer composite, J. Membr. Sci. 362 (2010) 374–383.
[31] P.S. Singh, V.K. Aswal, Characterization of physical structure of silica nanoparticles encapsulated in polymeric structure of polyamide films, J. Colloid Interface Sci. 326 (2008) 176–185.
[32] T.A. Saleh, V.K. Gupta, Synthesis and characterization of alumina nano-particles polyamide membrane with enhanced flux rejection performance, Sep. Purif. Technol. 89 (2012) 245–251.
[33] Y.J. Song, P. Sun, L.L. Henry, B.H. Sun, Mechanisms of structure and performance controlled thin film composite membrane formation via interfacial polymerization process, J. Membr. Sci. 251 (2005) 67–79.
[34] P.W. Morgan, Condensation Polymers: By Interfacial and Solution Methods, Interscience, New York, NY, 1965, pp. 20–30.
[35] G.Y. Chai, W.B. Krantz, Formation and characterization of polyamide membranes via interfacial polymerization, J. Membr. Sci. 93 (1994) 175–192.
[36] V. Freger, Nanoscale heterogeneity of polyamide membranes formed by interfacial polymerization, Langmuir 19 (2003) 4791–4797.
[37] V. Freger, Kinetics of film formation by interfacial polycondensation, Langmuir 21 (2005) 1884–1894.
[38] G.E. Mitchell, B. Mickols, D. Hernandez-Cruz, A. Hitchcock, Unexpected new phase detected in FT30 type reverse osmosis membranes using scanning transmission X-ray microscopy, Polymer 52 (2011) 3956–3962.
[39] F.A. Pacheco, I. Pinnau, M. Reinhard, J.O. Leckie, Characterization of isolated polyamide thin films of RO and NF membranes using novel TEM techniques, J. Membr. Sci. 358 (2010) 51–59.
[40] A.V. Berezkin, A.R. Khokhlov, Mathematical modeling of interfacial polycondensation, J. Polym. Sci. B: Polym. Phys. 44 (2006) 2698–2724.
[41] V. Freger, S. Srebnik, Mathematical model of charge and density distributions in interfacial polymerization of thin films, J. Appl. Polym. Sci. 88 (2003) 1162–1169.